University of Twente

Bachelor thesis

Applied Physics & Applied Mathematics

Extended Self Similarity in Rayleigh-Bénard Convection

Author:
Arnout Franken

Supervisors:
Ass. Prof. Dr. Richard Stevens (AP)
Prof. Dr. Ir. Bernard Geurts (AM)
MSc. Alexander Blass (Daily supervisor)

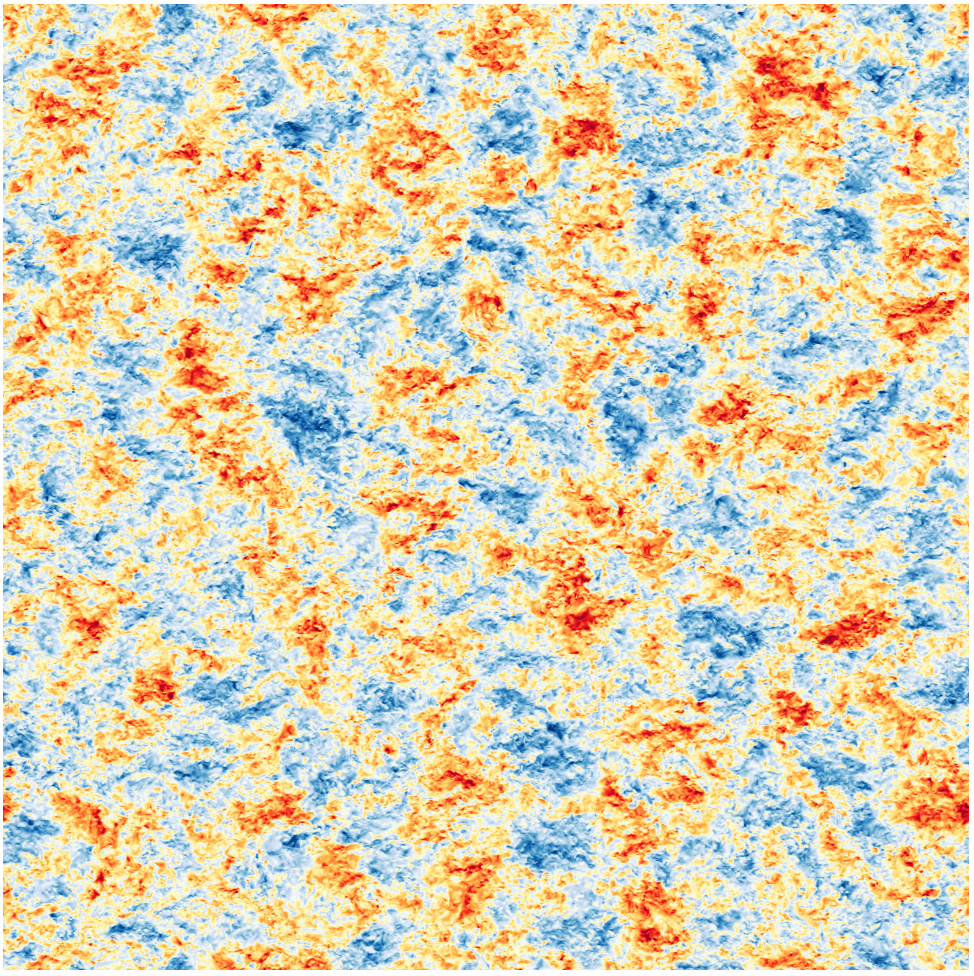

June 27, 2017

University of Twente

Abstract

TNW & EEMCS
PoF & MMS

Extended Self Similarity in Rayleigh-Bénard Convection

by Arnout Franken

The scaling behavior of the normalized even order structure functions $S_{2p}(r) = \left\langle (u(x+r) - u(x))^{2p} \right\rangle^{1/p}$ in various configurations of Rayleigh-Bénard (RB) convection is studied. Here u is a velocity component orthogonal to gravity, and x is the spatial coordinate component in the same direction. It is known that for shear driven wall-bounded flows, the longitudinal structure functions can be described by the self similar profile $S_{2p} \sim D_p \ln(r/y) + E_p$ in the logarithmic region, where y is the wall normal height and D_p and E_p are constants. In line with the extended self similarity hypothesis, it was recently shown that the ratios D_p/D_1 appear more universal. These ratios are extracted from plots between structure functions and show agreement for various shear flows. In this report, the above observations are tested for rectangular periodic RB convection cells with a width up to 64 times larger than the distance between the bottom and top wall. The self similar profile could not be observed for any of the different Raleigh number cases. The ratios D_p/D_1 however could clearly be found from the structure functions in the energy containing region of r. The values of D_p/D_1 were found not to be independent of wall normal distance. Compared to the previously found values in the logarithmic layer of shear flows, the ratios are lower near the bottom wall, and higher near the half height plane for RB convection. These results appear to be independent of the Rayleigh number in the range $Ra = 10^7 - 10^9$.

Contents

List of symbols

Symbol	Description
W	Width of flow domain
H	Height of flow domain, equal to 1
Γ	Aspect ratio of flow domain (W/H)
$\vec{\mathbf{x}}$	3-dimensional position in flow field, with $\vec{\mathbf{x}} \equiv (x, y, z)$
y	Wall normal distance; distance from bottom wall ($0 \leq y \leq 1$)
$\vec{\mathbf{u}}$	Velocity vector, where $\vec{\mathbf{u}} \equiv (u, v, w)$
u	$\vec{\mathbf{u}}$-component parallel to mean flow / one of the horizontal directions for RB convection
v	Velocity component antiparallel to gravity
T	Temperature
N	Number of grid points per horizontal dimension of flow field
n_t	Number of snapshots
n_r	Number of separation distances for calculating structure functions
n_y	Number of horizontal velocity slabs in data set
$p_{\max}$	Highest even order of structure functions that is calculated
S_{2p}	Normalized longitudinal velocity structure function of order $2p$
Ra	Rayleigh number
r	Spatial separation for structure functions
D_p	Scaling factor for the p^{th} structure function in the self similarity hypothesis
κ	Von Kármán constant

1 Introduction

This report describes a study done on structure function scaling in Rayleigh-Bénard convection. In this section, an introduction is given on the recent advances in the research on the statistical properties of wall bounded flows. This is followed by an introduction on Rayleigh-Bénard convection after which the research questions are postulated.

1.1 Background

In recent years, there has been an extensive study on the properties of turbulent flows. Specifically, many studies are carried out to determine universal statistical properties of wall bounded flows [1–5]. A robust feature of these turbulent flows is the *law of the wall*, which describes a logarithmic profile for the mean velocity. The law is described by:

$$\frac{\langle u \rangle}{u_\tau} = \frac{1}{\kappa} \ln y^+ + B, \tag{1}$$

where $\langle u \rangle$ is the time-averaged streamwise velocity, u_τ is defined as the wall friction velocity, $\kappa \approx 0.4$ is the Von Kármán constant and y^+ is the wall normal distance in wall units. This law describes a self similar profile for the mean velocity near a wall. Self similarity means that the profile retains its shape when the variable is scaled by some constant, so the scaled version is similar to itself.

More recently, there is also growing evidence for a self similar profile for the variance of the streamwise velocity fluctuations [4–6]. This law has the following form:

$$\left\langle (u'^+)^2 \right\rangle = A_1 \ln \frac{\delta}{y} + B_1, \tag{2}$$

where $u'^+ = (u - \langle u \rangle)/u_\tau$ is the normalized streamwise velocity fluctuation, δ is the outer length scale (for example boundary layer thickness or pipe diameter), $A_1 \approx 1.25$ is the Townsend-Perry constant, and B_1 is some constant of order 1 that depends on the flow configuration.

If the streamwise velocity fluctuations u'^+ are assumed to have a Gaussian distribution, then the higher order statistical moments obey similar laws [7]. For purely Gaussian statistics, the higher order moments scale as:

$$\left\langle (u'^+)^{2p} \right\rangle = (2p-1)!! \left\langle (u'^+)^2 \right\rangle^p, \tag{3}$$

where $n!! = n(n-2)(n-4)\cdots 1$ is the double factorial. Substituting this in equation 2 provides an expectation for the scaling of the higher order even moments of the velocity fluctuations:

$$\left\langle (u'^+)^{2p} \right\rangle^{1/p} = A_p \ln \frac{\delta}{y} + B_p. \tag{4}$$

The logarithmic trend was indeed experimentally confirmed [6, 7], but the scaling coefficients A_p are lower than predicted for Gaussian statistics, so $A_p < (2p-1)!!^{1/p} A_1$. Following the same analysis, De Silva [8] proposed that the logarithmic law should also hold for the longitudinal structure functions which are given by:

$$S_{2p}(r) \equiv \left\langle (u^+(x+r) - u^+(x))^{2p} \right\rangle^{1/p}. \tag{5}$$

When the structure function is evaluated at a fixed distance from the wall y^+ in the logarithmic region, and r in the streamwise direction, De Silva indeed experimentally found the logarithmic dependence predicted by the attached eddy-model [8]:

$$S_{2p} \sim D_p \ln \frac{r}{y} + E_p. \tag{6}$$

This result was further strengthened by data from Yang et al. [9] and De Silva [10]. Not only did they find this logarithmic dependence, they also found that the ratios D_p/D_1 appear to be universal. This result is in line with the extended self similarity hypothesis postulated first by Benzi *et. al.* [11]. He argued that not only do the structure functions have a particular scaling with r, there is also a universal scaling between different orders of structure functions in the inertial subrange (ISR) of r. His extended self similarity hypothesis for the ISR can be written as follows:

$$S_n \propto (S_3)^{2\xi_n/n}. \tag{7}$$

Here ξ_n is the anomalous scaling exponent, which will be described in more detail in section 2. The result from Yang *et al* and De Silva however showed that there is also extended self similarity on larger scales. This observation follows directly from equation 6 and the observation that D_p/D_1 appears universal:

$$S_{2p} \propto \frac{D_p}{D_1} S_2 - \frac{D_p}{D_1} E_1 + E_p. \tag{8}$$

This is the main equation for the research described in this report. In the remainder of this report, when the extended self similarity (ESS) hypothesis is mentioned, it discusses whether there is a universal scaling between the different orders of structure functions. The results from De Silva (2017) show a far reaching universality in the line of the ESS hypothesis in the energy containing region (ECR) of r in the form of equation 8, based on the currently investigated flow configurations.

1.2 Research questions

Up to now, the extended self similarity hypothesis in the ECR has only been tested for pressure driven flows. That is to say, flows where there is a mean velocity which is driven by a pressure gradient. The cases studied so far are boundary layer flows, pipe flows and channel flows [10]. An interesting question is therefore whether the ESS hypothesis in the ECR of r for longitudinal structure functions can also be found in convection flows. This result would be useful in understanding how the large and small scale motions interact [9].

One of the most widely studied cases of convection is Rayleigh-Bénard (RB) convection. It is a type of flow which develops in a fluid which is heated from below, and cooled from above by two unbounded horizontal surfaces. At the bottom wall, the fluid is heated, which causes it to expand. Due to the gravitational field, this slightly less dense fluid will rise up. At the same time, fluid at the top wall cools down, which causes it to move down.

An important dimensionless parameter for this flow is the Rayleigh number. It is defined as follows:

$$\mathrm{Ra} = \frac{g\beta\Delta T L^3}{\nu\alpha}, \tag{9}$$

where g is the gravitational acceleration, β is the thermal expansion coefficient of the fluid, ΔT is the temperature difference between the bottom plate and the top plate, L is the distance between the two plates, ν is the kinematic viscosity of the fluid, and α is its thermal diffusivity. The parameter Ra is a measure for the instability of the system. It is the ratio between the buoyancy force that makes the flow unstable, and the viscous force that has a stabilizing impact. A higher Rayleigh number will therefore mean that the flow is more turbulent [12].

An important length scale for RB convection is the Bolgiano length L_B. It is defined as:

$$L_B \equiv \frac{\epsilon^{5/4}}{(g\beta)^{3/2} N_T^{3/4}}, \tag{10}$$

where $\epsilon(\mathbf{x},t) \equiv \nu \left|\nabla \mathbf{u}(\mathbf{x},t)\right|^2$ is the turbulent kinetic energy dissipation rate and $N_T(\mathbf{x},t) \equiv \alpha \left|\nabla T(\mathbf{x},t)\right|^2$ is the temperature variance dissipation rate [13]. It represents the scale at which the buoyancy effects balance the viscosity effects in the equations of motion.

In this research, the structure function scaling as expressed in equation 8 will be investigated for Rayleigh-Bénard convection. In this configuration, the flow is driven by buoyancy instead of a pressure gradient. Another pronounced difference is that for RB convection, there is no mean velocity profile over the whole domain, so there is no preferred horizontal direction on large scales.

The question therefore arises whether the above observations of the self-similar and extended self-similar profiles will also hold for RB convection. If so, is there any dependence on the distance to the bottom/top wall?

This leads to the following research questions:

- **Self Similarity (SS)**: Do the structure functions for Rayleigh-Bénard flow show the same logarithmic profile (equation 6) as for the pressure driven flows?
- **Extended Self Similarity (ESS)**: Can the results for the structure function ratios D_p/D_1 (equation 8) for pressure driven flows be generalized to include flows driven by natural convection at different wall normal distances?

1.3 Outline

The outline for this report is as follows. In section 2, known scalings of the structure functions for various domains will be discussed to serve as a reference for verifying the results. Section 3 contains a description of the methods used to calculate the structure functions. The results of these methods are shown in section 4, which will be discussed in section 5. A conclusion will be given in section 6. Finally, section 7 contains recommendations for further research.

2 Theory

According to the self similarity hypothesis, the longitudinal structure functions will scale proportional with $\ln(r/y)$ in the logarithmic region [10]. However, to check if the structure functions are calculated correctly, the results can be compared to known scalings in different regions. These scalings will be discussed in the following sections.

2.1 Very small scales (dissipation range)

We assume that the velocity field is at any time a continuous, differentiable function of space. This means that the longitudinal velocity field has a Taylor expansion, given by:

$$u(\vec{\mathbf{x}} + r\hat{\vec{\mathbf{e}}}_1) = u(\vec{\mathbf{x}}) + r\frac{\partial u}{\partial x_1}(\vec{\mathbf{x}}) + \frac{r^2}{2}\frac{\partial^2 u}{\partial x_1^2}(\vec{\mathbf{x}}) + \ldots, \tag{11}$$

where the 1-direction is the longitudinal direction. Substituting this into the expression for the structure functions in equation 5 and taking the limit for $r \to 0$ gives:

$$\lim_{r\to 0} S_{2p}(r) = \left\langle \left(r\frac{\partial u}{\partial x_1}(\vec{\mathbf{x}}) \right)^{2p} \right\rangle^{1/p} \quad \to \quad S_{2p} \sim r^2 \quad \text{for } r \to 0. \tag{12}$$

So for very small values of r, the scaling as r^2 should appear in the structure functions [8].

2.2 Small scales (inertial sub-range)

A lot of research has been done on structure function scaling in the inertial sub-range for homogeneous isotropic flows [14]. The scaling in the ISR is expressed as:

$$\langle (u(\vec{\mathbf{x}} + r) - u(\vec{\mathbf{x}}))^n \rangle = C_n(\epsilon r)^{n/3} \left(\frac{r}{\ell}\right)^{\xi_n - n/3}, \tag{13}$$

where ℓ is the length scale and ξ_n is the anomalous scaling exponent. Rewriting this to get a scaling for the compensated structure functions S_{2p} gives the following scaling [8]:

$$S_{2p} \sim \left(\frac{r}{y}\right)^{\xi_{2p}/p}. \tag{14}$$

The Kolmogorov 1941 theory (K41) predicts $\xi_n = n/3$. Experimental data shows that $\xi_n < n/3$ for $n > 3$ [14]. In stead, it follows the She-Leveque model quite well [15], which is given by:

$$\xi_n = \frac{n}{9} + 2\left[1 - \left(\frac{2}{3}\right)^{n/3}\right]. \tag{15}$$

The numerical values for the scaling exponents for the structure functions ($n = (2, 4, 6, 8, 10)$) are therefore given by the She-Leveque model as: $\xi_n = (0.696,\ 1.280,\ 1.778,\ 2.211,\ 2.593)$. To see the difference with the prediction from the K41 theory, both models are shown in figure 1. The scaling from equation 14 with these exponents are expected to be present in the structure functions at scales between the dissipation range and the Bolgiano length L_B [13].

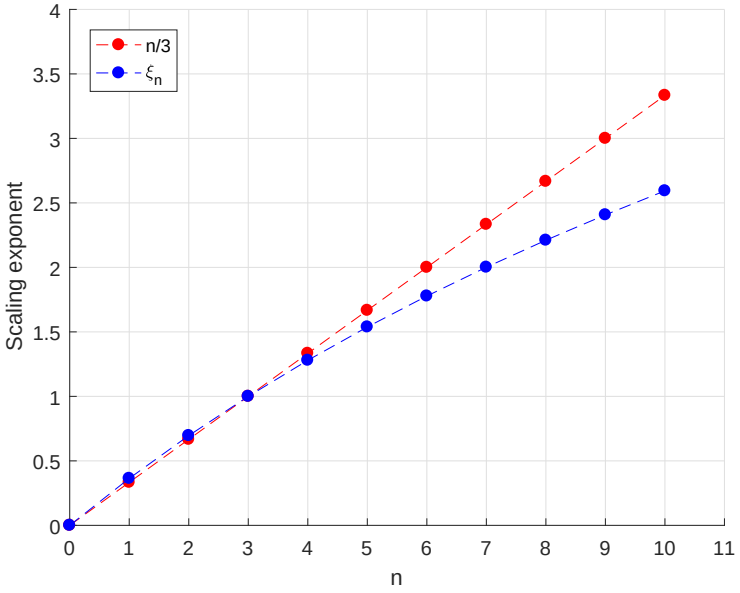

Figure 1: Scaling exponents given by the K41 theory (red dots) and by the She-Leveque model (blue dots) up to the tenth order. The She-Leveque model predicts lower scaling exponents for the higher order structure functions.

2.3 Large scale limit

At the other end of the spectrum we have discussed so far, the large values of r, the second order structure functions will approach a constant value. This becomes clear when we recall the definition of the longitudinal structure functions:

$$S_{2p}(r) = \left\langle (u(\vec{\mathbf{x}} + \vec{\hat{e}}_1) - u(\vec{\mathbf{x}}))^{2p} \right\rangle^{1/p}. \tag{16}$$

The first thing to note is that for large values of r, the velocity at two points at distance r from each other will be uncorrelated [8]. Secondly, there is no preferred direction in the horizontal plane, so the mean horizontal velocity is zero. This can be used to simplify the second order structure function:

$$\begin{aligned} S_2(r) &= \left\langle u^2(\vec{\mathbf{x}} + r\hat{\mathbf{e}}_1) - u(\vec{\mathbf{x}} + r\hat{\mathbf{e}}_1)u(\vec{\mathbf{x}}) + u^2(\vec{\mathbf{x}}) \right\rangle \\ &= \left\langle u^2(\vec{\mathbf{x}} + r\hat{\mathbf{e}}_1) \right\rangle - \left\langle u(\vec{\mathbf{x}} + r\hat{\mathbf{e}}_1)u(\vec{\mathbf{x}}) \right\rangle + \left\langle u^2(\vec{\mathbf{x}}) \right\rangle. \end{aligned} \tag{17}$$

Since the angle brackets $\langle \cdot \rangle$ denote an ensemble average, the second term in equation 17 has to be zero. This is because $u(\vec{\mathbf{x}} + r\hat{\mathbf{e}}_1)$ and $u(\vec{\mathbf{x}})$ are independent, so:

$$\left\langle u(\vec{\mathbf{x}} + r\hat{\mathbf{e}}_1)u(\vec{\mathbf{x}}) \right\rangle = \left\langle u(\vec{\mathbf{x}} + r\hat{\mathbf{e}}_1) \right\rangle \left\langle u(\vec{\mathbf{x}}) \right\rangle = 0. \tag{18}$$

Because of independence, the first and third term in equation 17 are equal, so the final result is:

$$S_2(r) \to 2\left\langle u^2 \right\rangle \quad \text{for} \quad r \to \infty. \tag{19}$$

This means that the second order structure function will approach twice the variance when r is large enough [8].

Summary

The structure functions are expected to show three different scaling behaviors in different regions. Below is an overview of those scalings.

- $\mathbf{r \approx 0}$: $S_{2p}(r) \sim r^2$
- **ISR**: $S_{2p}(r) \sim r^{\xi_{2p}/p}$
- $\mathbf{r \to \infty}$: $S_{2p}(r) = 2\left\langle u^2 \right\rangle$

3 Methods

3.1 Available data sets

For this research, a database is used with simulations of RB convection [16]. All simulations use a rectangular convection cell of vertical height H and width W for the two horizontal dimensions. To approximate an infinite domain in the horizontal directions, the vertical boundaries are chosen periodic. At the top and bottom, the fluid is contained by a wall. The heigt of the domain H is set equal to 1, such that the wall normal distance y is between 0 (bottom) and 1 (top). The database contains simulations for different Ra numbers and different aspect ratios $\Gamma \equiv W/H$. A complete list of the different simulations is shown in table 1.

Table 1: Database of simulations of RB instabilities for different Ra numbers and aspect ratios. The temperature and velocity data are available on n_y horizontal cross-sections, containing an equally spaced grid of dimensions $(N \times N)$. For each cross-section, there are n_t snapshots available.

Ra	Γ	n_t	Grid size $(N \times N)$	n_y
2×10^7	3	1000	384×384	1
2×10^7	4	1000	512×512	1
2×10^7	8	1000	1024×1024	1
2×10^7	16	999	2048×2048	1
2×10^7	32	1105	4096×4096	1
2×10^7	64	600	8192×8192	1
1×10^8	3	365	576×576	8
1×10^8	4	500	768×768	8
1×10^8	8	309	1536×1536	8
1×10^8	16	475	3072×3072	8
1×10^8	32	553	6144×6144	8
1×10^8	64	167	12288×12288	8
1×10^9	2	2683	768×768	8
1×10^9	3	937	1152×1152	8
1×10^9	4	500	1536×1536	8
1×10^9	8	1980	3072×3072	8
1×10^9	16	1144	6144×6144	8
1×10^9	32	278	12288×12288	8

As seen in table 1, there are simulations of RB convection for very large aspect ratios, indicating a domain that is much wider than its height. The reason for this is that the flow contains structures with a size of several times the domain height [17]. To ensure that these structures are well resolved in the simulation, the flow domain must ideally have an aspect ratio that is several times larger than the largest structures [16]. In the next section, the energy spectra will be used to confirm that this criterium holds for the largest aspect ratio cases.

However, a larger aspect ratio also means a larger dataset. For example, the data where $Ra = 10^8$ and $\Gamma = 64$ is several terabytes in size. For this reason, the data analysis will be performed on Cartesius. This is the Dutch national supercomputer located in Amsterdam, at which MATLAB scripts can be executed.

3.2 Calculating structure functions on Cartesius

The goal is to calculate the longitudinal structure functions, which are defined as:

$$S_{2p}(r) = \left\langle \left(u(\vec{\mathbf{x}} + r\hat{\mathbf{e}}_{\mathbf{1}}, t) - u(\vec{\mathbf{x}}, t)\right)^{2p} \right\rangle_{A,t}^{1/p}, \tag{20}$$

where the subscript A indicates an average over a horizontal plane, and the subscript t indicates a time average. The 1-direction is in the direction of u. Technically, these are called the compensated structure functions, but they will simply be referred to as the structure functions.

This equation can be directly applied to the velocity field in RB turbulence. There is data available at a few different wall normal distances. In other words, the velocity field is known at a few horizontal slabs of the domain. For each slab, the data is available as an (NxN) grid for each snapshot.

For the first analysis, which is done on Cartesius, the structure functions are calculated for each time separately. Later on, this data is further processed by taking a time average. Therefore, on Cartesius the following quantities are calculated:

$$S_{\text{uncompensated}}(r,p,t) = \left\langle (u(\vec{\mathbf{x}} + r\hat{\mathbf{e}}_{\mathbf{1}}, t) - u(\vec{\mathbf{x}}, t))^{2p} \right\rangle_A . \tag{21}$$

3.2.1 Code development

The main analysis can be captured in pseudo code as follows:

```
1  for slab = ⟨every cross-section⟩
2     % Pre-define matrix for uncompensated structure functions
3     for j = ⟨every snapshot⟩
4        % Read velocity data from database
5        for r = ⟨every separation distance⟩
6           % Calculate S_uncompensated
7        end
8        % Calculate mean velocity
9        % Calculate variance
10    end
11    % Save structure function data
12 end
```

Figure 2: Pseudo code for calculating uncompensated structure functions on Cartesius

The first step in calculating the uncompensated structure functions from equation 21 is to calculate the velocity differences. This process is shown graphically in figure 3. The velocity field is first duplicated. The matrix is then split up at the point r_k, which represents the k^{th} column.

To obtain the velocity field $u(x + r_k)$, the matrix columns are simply reordered by first taking the last $(N - k)$ columns and then extending it with the first k columns. This can only be done because the boundaries are periodic. Then finally, the original matrix is subtracted from it to obtain the quantity $(u(x + r) - u(x))$, which is subsequently squared point-wise.

In MATLAB, this process is done in one line.

```
1  diffu2 = (u - u(:,[r:end,1:r-1])).^2;
```

After that, this velocity difference is used to calculate the different orders of structure functions. This is done iteratively in a `for`-loop, and is shown graphically in figure 4. The spatial averaging is done by taking the mean of the matrix with the velocity differences.

As shown on line 9 of the pseudo code in figure 2, the variance is also calculated. This is later on used to determine the limiting value of the structure functions for large values of r. The variance is given by $\langle u^2 \rangle$. In MATLAB, this looks as follows:

```
1  Intensity(j) = mean(mean(u.*u));
```

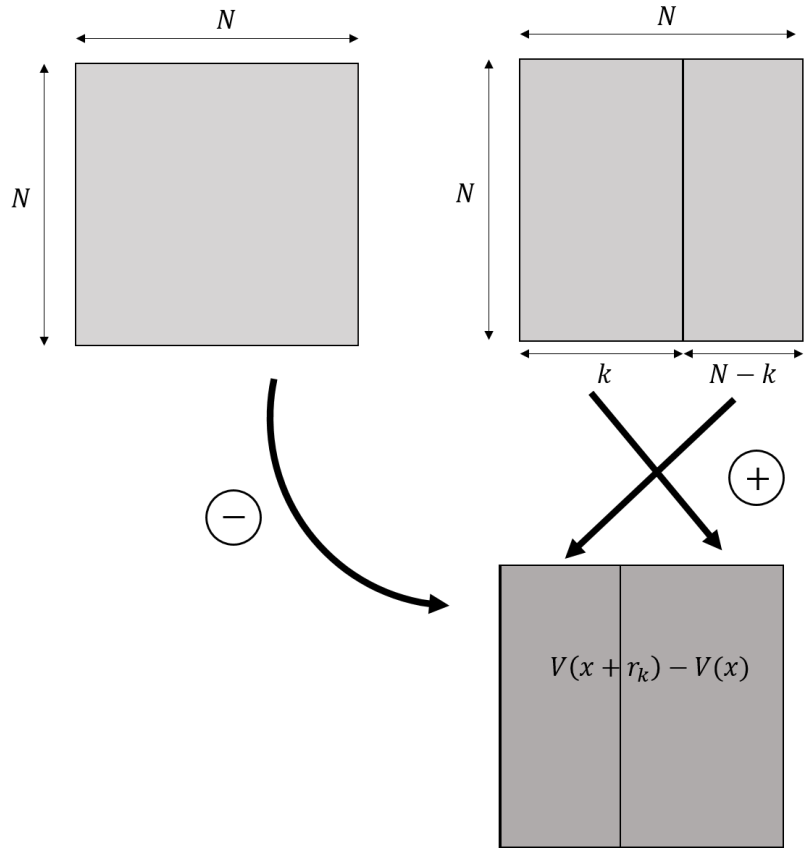

Figure 3: Graphical representation of the operation done to calculate the velocity differences. The step of placing the last $N-k$ columns of the velocity field on the left side is only possible because of periodic boundary conditions.

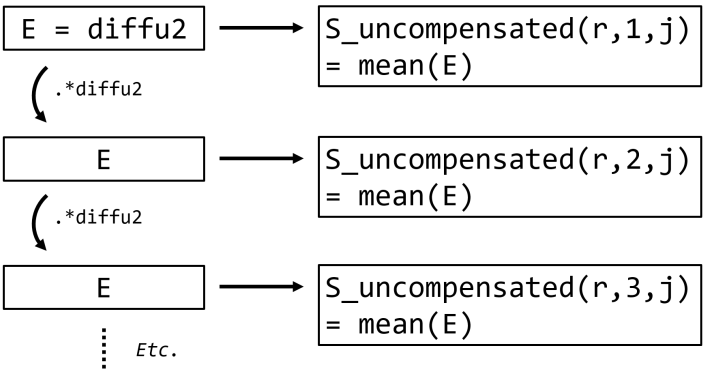

Figure 4: Graphical representation of the iterative process to calculate higher order structure functions.

This process is done for every available slab. Finally, the output of the code is a file for every slab which contains a matrix of size $(N \times p_{max} \times n_t)$ corresponding to equation 21, and an array for the variance at every snapshot.

3.2.2 Computational costs

Even though the process of calculating the structure functions is quite simple and straighforward, it requires a large amount of computations due to the size of the data.

The code contains 4 nested `for`-loops; over all slabs, snapshots, seperation distances and orders of the structure functions. The process shown in figure 4 involves $2 \times p_{max} \times N^2$ multiplications and

$(p_{max}+1) \times N^2$ additions when also accounting for the fact that DIFFU2 (see figure 4) has to be calculated.

By setting the number of seperation distances r that are used to n_r, an estimate can be made for the total number of computational operations. Taking into account all `for` loops, we need $n_y \times n_t \times n_r \times (3p_{max}+1) \times N^2$ operations.

The biggest case was for $Ra = 10^8$, $\Gamma = 64$. Using the values from table 1 and setting $n_r = 100$ and $p_{max} = 5$, the number of operations for processing this data set is approximately 3×10^{14}. On Cartesius, this task took about 6 hours to complete using 24 CPUs. Since the three `for` loops in figure 2 have independent iterations, they can be executed parallel on the different CPUs. To do this, the `for` statement in line 3 is changed to `parfor`, so the iterations over all snapshots is distributed over the cores.

In an ideal scenario, the structure functions would be calculated for every possible separation distance, so $n_r = N$. This is done for the smaller datasets ($N \leq 1536$), however it was not feasible for the larger data sets due to the computation time. Therefore, only about 100 values of r were selected such that the structure functions are still sufficiently smooth. This was done by choosing them equally spaced on a logarithmic axis between 1 and N as can be seen later on in figure 7.

3.3 Convergence analysis

The output of the code submitted to Cartesius is the uncompensated structure functions for every snapshot. In accordance with equation 20, this data has to be averaged over time, and raised to the power $1/p$ to obtain the compensated structure functions.

The first problem with this is that the flow is possibly not yet in statistical equilibrium during the first few snapshots. This can be easily seen when looking at the Nusselt number for every snapshot. The Nusselt number Nu is defined as the ratio of the total and conductive heat flux. The time series of Nu gives a good estimation as to whether the system is in a statistical equilibrium or not. An example of this is shown in figure 5. In this case, the first ~ 50 time frames will simply be discarded since they are heavily influenced by initial conditions. After that, the Nusselt number is in a statistical equilibrium.

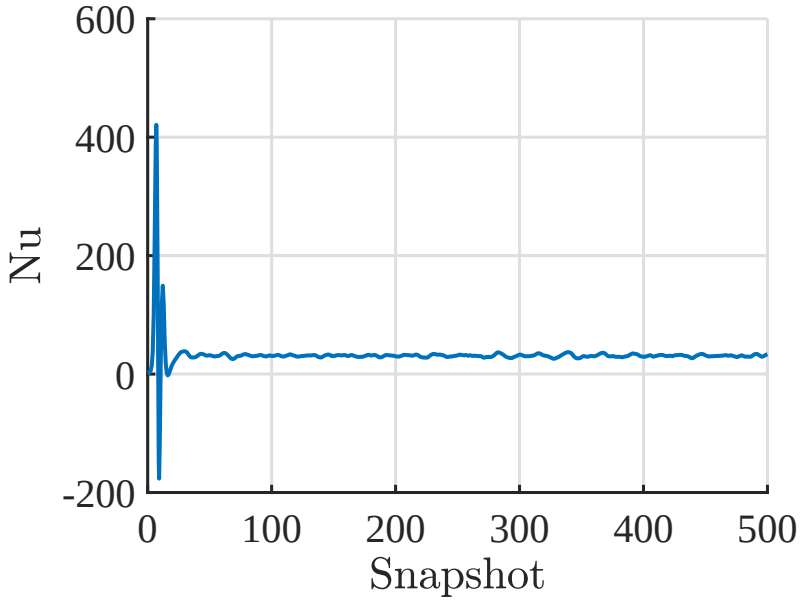

Figure 5: Nusselt number as function of time for $Ra = 10^8$ and $\Gamma = 4$. The Nusselt number is in statistical equilibrium after the first ~ 50 snapshots.

We are now left with only the snapshots where the flow is in statistical equilibrium. The uncompensated SFs will however still fluctuate between snapshots due to the chaotic nature of the flow. This means that

the temporal averaging is associated with a confidence interval. A code from Gijs Kooij (Department of Applied Mathematics) is used to calculate the standard error of a dataset $(\mathbf{t}, \mathbf{x})$.

Since we have time-correlated data, the code first calculates the lag time τ. For this, the code calculates the auto-correlation function, given by:

$$r(\tau) = \frac{\langle (x(t) - \mu)(x(t+\tau) - \mu) \rangle_t}{s^2}, \tag{22}$$

where it is normalized such that $r(0) = 1$. When the correlation function drops below a threshold, say $r(\tau) = 0.2$, then the data is approximately uncorrelated after time τ. By resampling the data with τ as the new timestep, we obtain an uncorrelated set of sample for which the mean and the standard error can be calculated. If we assume the uncorrelated data to be normally distributed, then the 95%-confidence interval is given by 1.96 times the standard error.

3.4 Structure function ratios

Using the methods described above, we can check if there is a self-similar profile for the longitudinal structure functions. Reciting equation 6, we have seen that for pressure driven flows, the structure functions scale as:

$$S_{2p} \sim D_p \ln \frac{r}{y} + E_p, \tag{23}$$

in the logarithmic region. Furthermore, the ratio D_p/D_1 appeared to be universal, leading to the extended self similarity hypothesis. These ratios can be determined by looking at the ratio between structure functions. In particular, rewriting equation 23 gives the following:

$$S_{2p} = \frac{D_p}{D_1} S_1 + E_p - \frac{D_p}{D_1} E_1. \tag{24}$$

This seems to indicate that D_p/D_1 can be easily calculated as the slope of the linear fit when plotting S_{2p} as a function of S_1. Note that equation 24 is a general result in case the structure functions can be written in the form:

$$S_{2p} \sim D_p f(r, y) + E_p, \tag{25}$$

where f is an arbitrary function. This seems to indicate that the extended self similarity could hold even when the structure functions do not show the logarithmic self-similar profile.

3.5 Summary

To summarize the analysis performed to calculate the structure function ratios, the list below shows all the steps taken.

1. Calculate uncompensated structure functions and variance of velocity field for every snapshot on Cartesius.
2. Determine the snapshot after which the flow is in statistical equilibrium using the Nusselt number.
3. Calculate the temporal mean and corresponding standard error of the uncompensated structure functions.
4. Calculate compensated structure functions and corresponding 95%-confidence intervals.
5. Determine structure function ratios D_p/D_1 using a linear fit on S_{2p} as function of S_2.

4 Results

Using the methods described in section 3, the compensated structure functions are calculated for every dataset in table 1. First, a comparison between different aspect ratio cases will be shown. After that, the structure functions will be tested for their expected scaling in different regions. Next, the ratios between different orders of the structure functions will be determined to obtain the ESS coefficients D_p/D_1. These final results will be compared for different Rayleigh numbers and wall normal distances.

4.1 Dependence on aspect ratio

For every Rayleigh number, there are data sets for different domain sizes. These sizes are characterized by the aspect ratio, which is the ratio between the horizontal length of the convection cell and the height of the cell. Obviously, structures larger than the domain size can not be observed in the simulation.

Figure 6 shows the second order structure function for $Ra = 10^8$ at wall normal distance $y = 0.15$ for different aspect ratios. For small separation distances, the results are very consistent. This means that the flow is similar at the smaller scales. For the larger separations, there is a large difference between the different aspect ratio cases. The nature of this will be adressed in the next section.

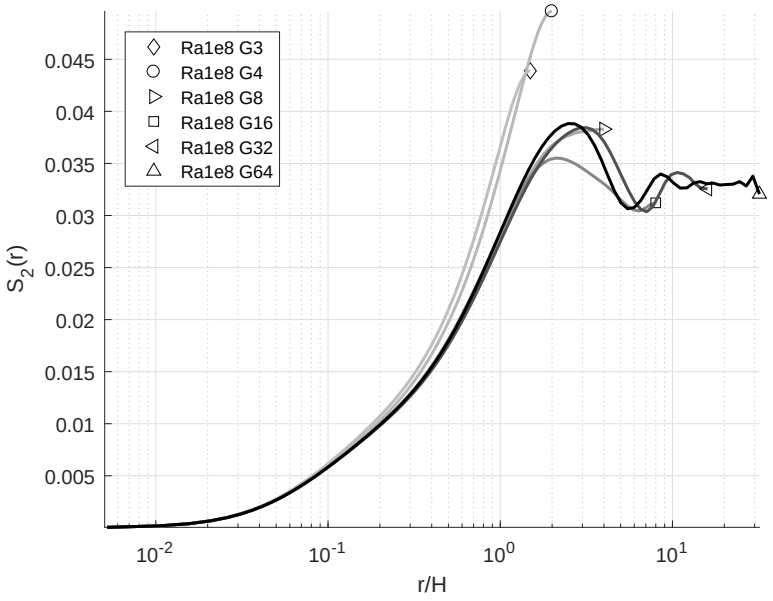

Figure 6: Second order velocity structure function for Ra= 10^8 for different aspect ratios, all taken from the slab where $y = 0.15$.

4.2 Large scale structures

The expectation for large values of r is that the structure functions limit to a constant value. This is observed in figure 6 only for the case where $\Gamma = 64$, however not for the smaller aspect ratio cases. Interestingly though, all structure functions show an oscillating behavior, which seems to have a maximum for $r \approx 2.5H$. This is shown more clearly in figure 7, where the structure function for the $Ra = 10^8$, $\Gamma = 64$ case is shown at different wall normal locations.

Physically, these local maxima mean that the velocity at one point in the flow is negatively correlated to the velocity at a distance $r \approx 2.5H$. A local minimum is observed at $r \approx 5 - 6H$, which indicates that the velocity at one point is positively correlated to the velocity at that distance.

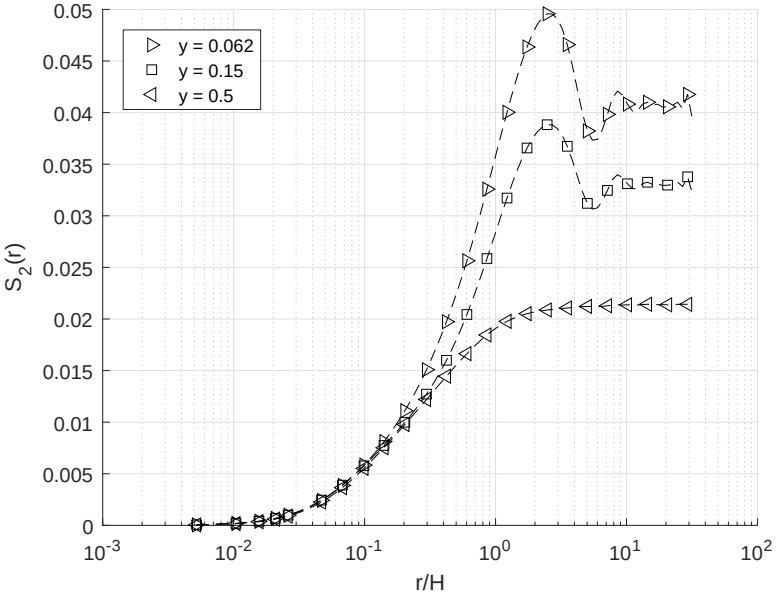

Figure 7: Second order velocity structure function for Ra= 10^8, $\Gamma = 64$. For clarity, only a quarter of the actual datapoints are plotted.

These observations hint at structures of size $(5-6)H$. This can be checked when looking at the energy spectrum for the velocity field. The spectrum is shown in figure 8 for the different wall normal locations from figure 7.

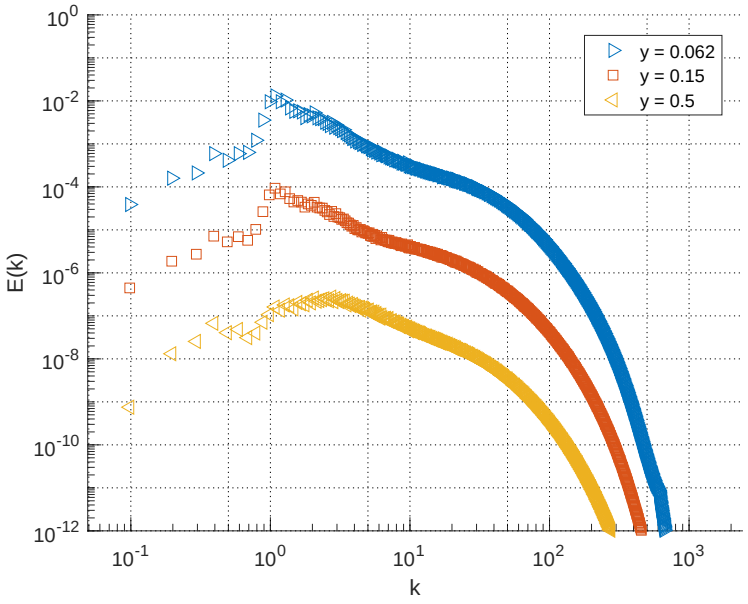

Figure 8: Kinetic energy spectrum at different wall normal locations y, all for the case where $Ra = 10^8$ and $\Gamma = 64$ [16]. The spectrum for $y = 0.15$ and $y = 0.5$ are shifted downwards two and four decades respectively for clarity.

The energy spectrum for the slabs closer to the bottom wall show a clear peak at $k_{max} = 1.08$. This corresponds to a wavelength of $\lambda_{max} = 2\pi k_{max} \approx 5.8H$, indicating structure of that size. The result is in good agreement with that structure size determined from the structure functions.

The existence of those large scale structures is the reason why, for the next sections, only the large aspect

ratios cases are shown. This ensures that the dynamics of these structures are taken into account when looking at the (extended) self similarity profiles [16].

4.3 Structure function scaling

The structure functions seem to be consistent for different aspect ratios, and they show the large scale structure. In this section, the structure functions will be analyzed to see whether they show the predicted scalings from section 2.

4.3.1 Very small scales (dissipation range)

For very small separation distances r, the second order structure functions are predicted to scale as $S_2(r) \sim r^2$. Figure 9 shows a plot of S_{2p}/r^2 for different orders p and wall normal distances y. The data is consistent for the different values of y, and the scaling of r^2 is visible for all orders of the structure functions.

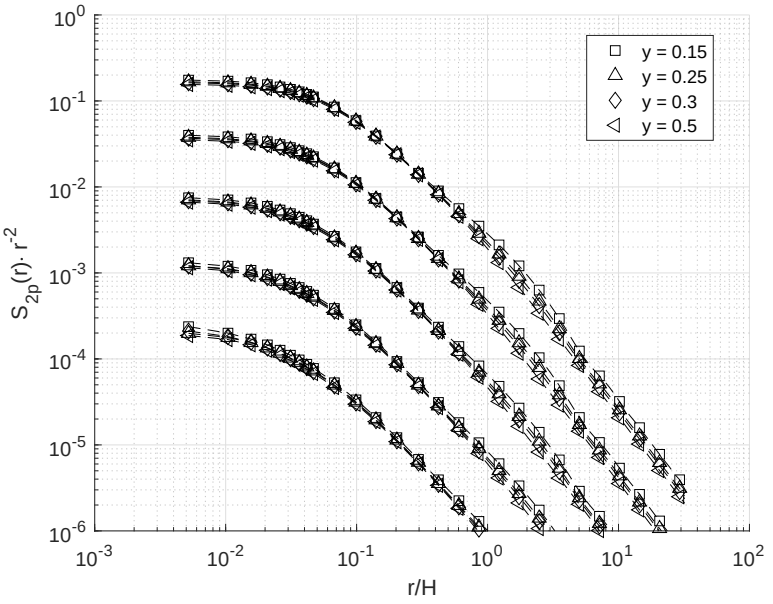

Figure 9: Velocity structure functions for Ra= 10^8, $\Gamma = 64$ at four different wall locations y, compensated by the expected scaling $S_{2p} \sim r^2$. The different even orders of the structure functions are shown from top ($p = 1$) to bottom ($p = 5$). The structure functions indeed scale as expected for the smallest values of r.

4.3.2 Small scales (inertial sub-range)

In the inertial subrange, the structure functions are expected to follow the scaling given by the exponents from the She-Leveque model as introduced in the previous sections. The scalings $S_{2p} \sim r^{\xi_{2p}/p}$ are shown in figure 10 for different values of p at four different wall normal locations y.

As shown in the figure, the expected scaling is observed in the range from $r \approx 0.08$ to $r \approx 1$, depending on wall normal location. For structure functions closer to the bottom wall, the regime for She-Leveque scaling is largest.

4.3.3 Large scale limit

For the largest values of r, the structure functions are expected to limit to twice the variance $\langle u^2 \rangle$. The structure functions for the case with $Ra = 10^8$, $\Gamma = 64$ are shown in figure 11 at different wall normal

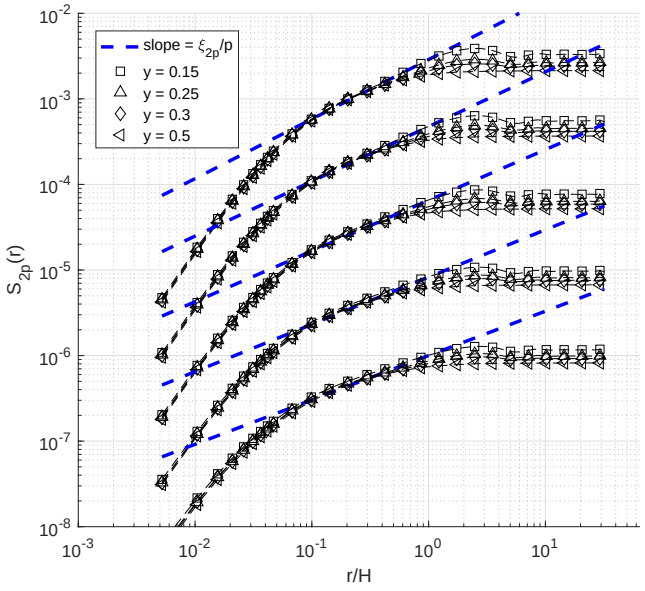

Figure 10: Velocity structure functions for Ra= 10^8, $\Gamma = 64$ at different wall normal locations y. From top to bottom are the different orders of structure functions from $p = 1$ (top) to $p = 5$ (bottom). Every order is shifted down an extra decade for clarity. The blue line indicates the scaling exponent predicted by the She-Leveque model [15].

locations. They seem to converge to the expected value as the oscillating behaviour dies out for larger values of r.

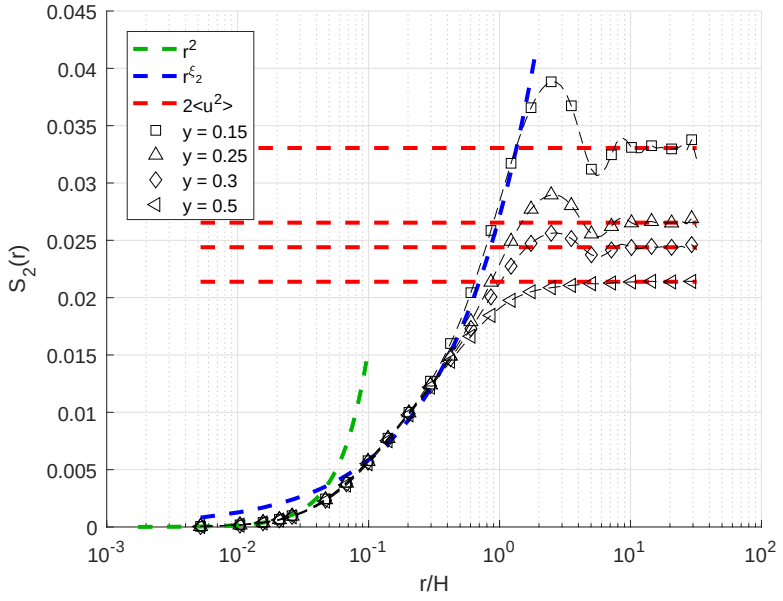

Figure 11: Second order velocity structure function for $Ra = 10^8$, $\Gamma = 64$. The red lines indicate the independently calculated limiting values of $S_2(r)$ for $r \to \infty$. In green and blue, the scalings from the previous sections are shown.

4.4 Structure function ratios

All structure functions show the expected scalings in different regimes. However, the structure functions do not show the expected self similarity profile given by equation 6 in the introduction. As shown in figure 12, the structure functions do not show any collapse to a universal profile at all when plotting as function of r/y.

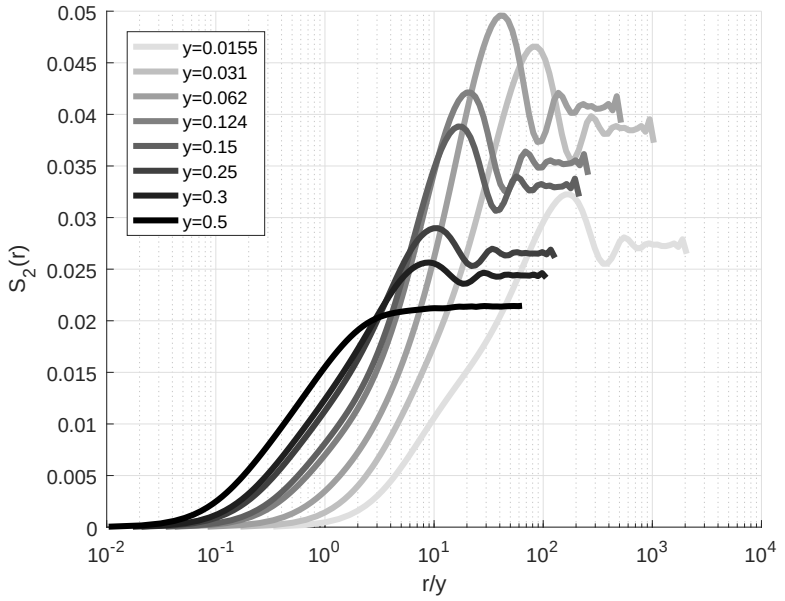

Figure 12: Structure functions at different wall normal locations for $Ra = 10^8$, $\Gamma = 64$. The data closer to the boundary has a lighter color. According to equation 6, this plot should show a universal profile with a linear part.

Even though the self similarity does not seem to be present these Rayleigh-Bénard flow simulations, we can still check for the extended self similarity. For that, the different orders of structure functions will be compared to see if they scale linearly with each other.

For this analysis, the simulations with the highest aspect ratios are used, since they also capture the large scale structures well. The structure functions for these cases are also better converged, since the large domains imply better spatial averaging.

Table 2 shows the higher even order structure functions as a function of the second order structure functions. The plots are given for three different wall normal locations y. The lower right graph shows the slopes of the linear fits for five different values of y. As a comparison, the slopes found by De Silva (2017) [10] are plotted. There is also an expectation for Gaussian statistics. If the velocities are assumed to be normally distributed, then the limiting value of the structure functions is known. When r is large enough such that the velocities at that distance are uncorrelated, then the Gaussian statistics give the result $S_{2p}/S_2 = ((2p-1)!!)^{1/p}$ similar to equation 3 from the introduction. To get an estimation for the structure for smaller values of r, we assume that the structure has the same shape as the calculated curves shown in table 2 but scaled as to fit the Gaussian prediction in the large r-limit. Finally, the prediction for Gaussian statistics of the ratios D_p/D_1 is given by determining the slope of this scaled version of the structure functions.

Table 2 shows that the extended self similarity coefficients D_p/D_1 are not universal for every wall normal distance y. The graph clearly indicates that the coefficients increase when y gets closer to the half-height plane. Also, for $y \to 0.5$, the results for D_p/D_1 get very close to the prediction for Gaussian statistics.

This can be seen directly in the statistics of the velocity field for the different slab heights. Figure 13 shows the probability density function of the horizontal velocity at three different values of y. In red, a Gaussian fit is plotted for every slab height. For the case with $y = 0.5$, the statistics are very close

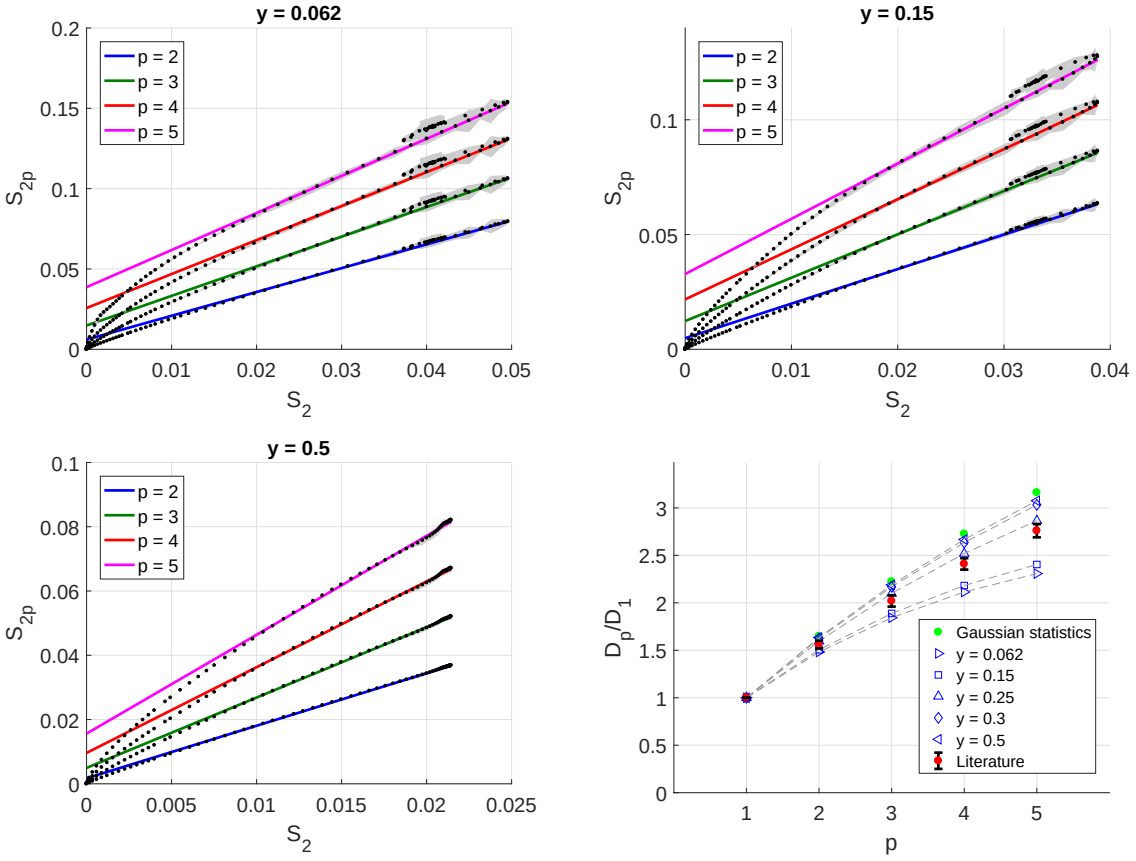

Table 2: Extended Self Similarity profiles at three out of eight different wall normal distances y, for the data set where $Ra = 10^8$, $\Gamma = 64$. The solid lines correspond to a first order polynomial fit with outliers excluded. The slopes are collected in the lower right graph. The grey bands represent the 95%-confidence intervals. The literature data indicate the data taken from De Silva (2017) [10] in the logarithmic region for pressure driven flows

to Gaussian, especially for the small velocities. Closer to the bottom wall, the statistics deviate more from their Gaussian fits. The probability of high velocities is lower than for Gaussian statistics. For the high order structure functions, rare events have a large contribution, since it uses the u^{2p}. Therefore, if rare events are less frequent, the ratio between high order SFs and the second order SF will be lower compared to the Gaussian statistics. This explains why the ratios D_p/D_1 are higher near the half-height plane and get closer to the Gaussian prediction, since the PDFs get more similar to a normal distribution with more frequent rare events.

Even though the results for the extended self similarity are in general different from the values from De Silva, they are very close for $y \approx 0.2$. This is better shown in figure 14, where the same data as in table 2 is displayed, but as a function of wall normal location y as opposed to p. In this figure, the red bands indicate the data taken from De Silva (2017). The curves from the Rayleigh-Bénard structure functions intersect with the literature data at $y \approx 0.2$.

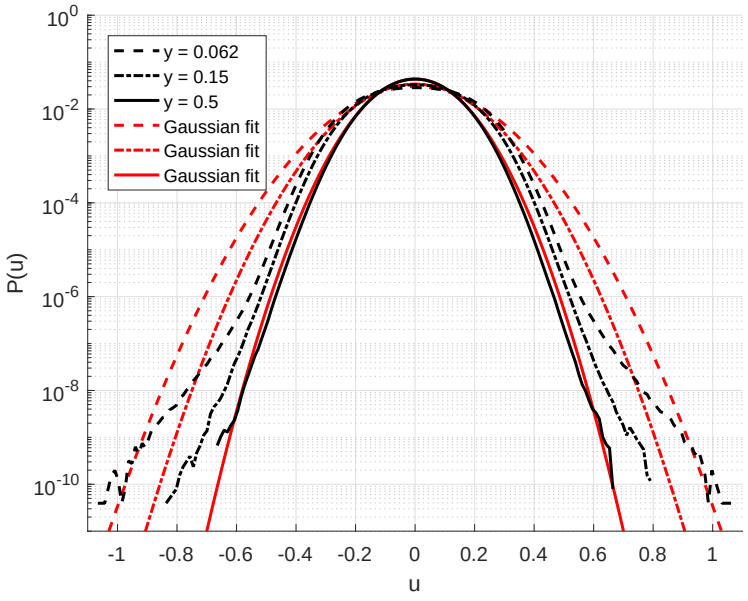

Figure 13: Probability Density Functions (PDFs) of the horizontal velocity at different wall normal distances y. For this data, $Ra = 10^8$ and $\Gamma = 64$.

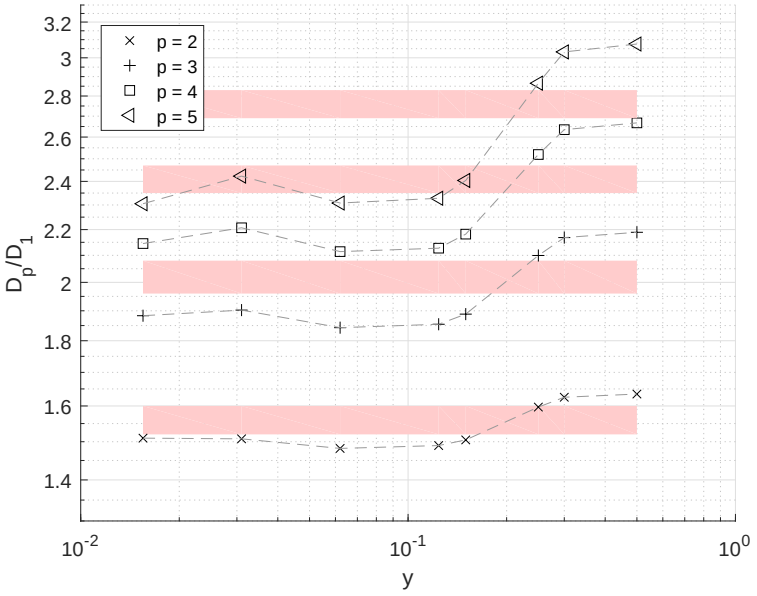

Figure 14: ESS slopes D_p/D_1 as a function of wall normal distance y. For this data, $Ra = 10^8$ and $\Gamma = 64$. The red bands indicate the data from Da Silva (2017), which included only data in the logarithmic region.

4.5 Rayleigh number dependence

Since there is data for various values of the Rayleigh number, it is interesting to check whether the previous results for the structure function ratios are independent of Rayleigh number. Tabel 3 shows the results for three different Rayleigh numbers, where $\Gamma = 16$. The data for $Ra = 10^8$ and $Ra = 10^9$ show the same trend for the y-dependence of the SF ratios. For the case with $Ra = 2 \times 10^7$, only data at $y = 0.5$ is taken.

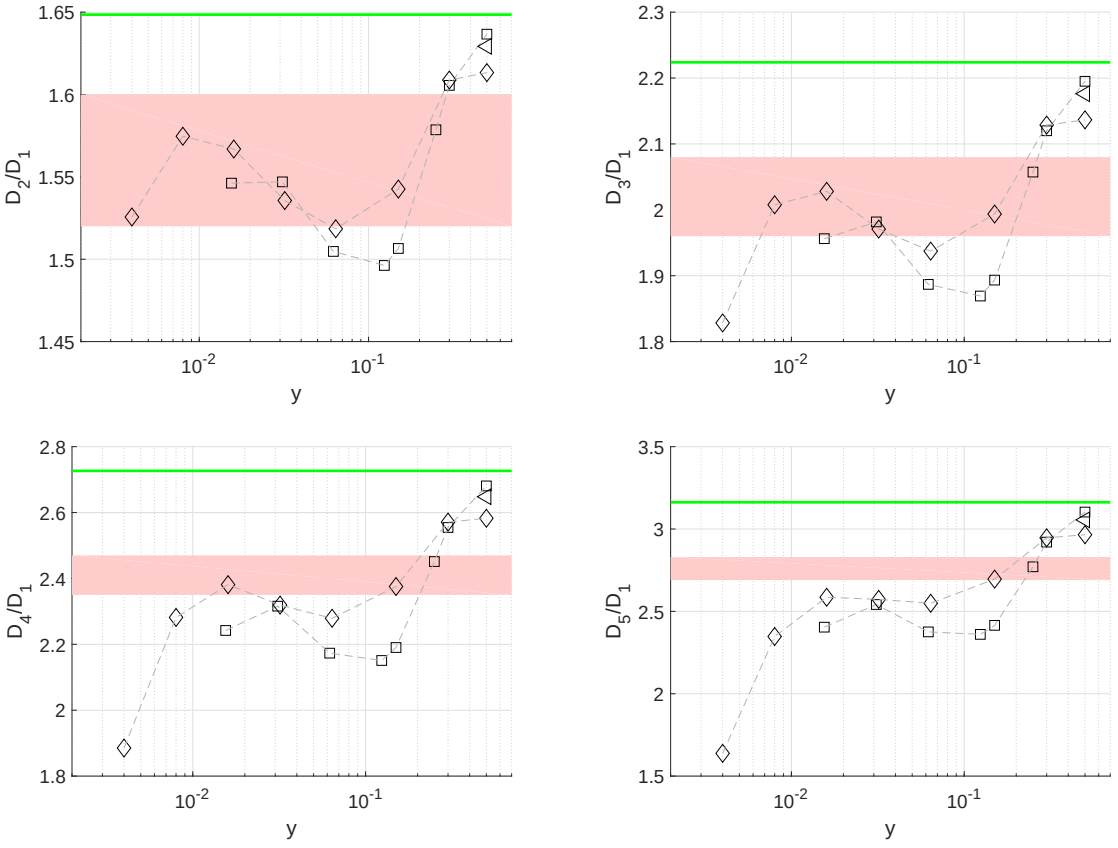

Table 3: Extended Self Similarity for different orders of the structure functions. The triangular markers (◁) indicate the $Ra = 2 \times 10^7$ data, squares (□) indicate $Ra = 10^8$ data and diamond shaped markers (◊) indicate $Ra = 10^9$ data. The green lines are the expectations for Gaussian statistics. For all data, $\Gamma = 16$. The red bands indicate the data from De Silva (2017) [10] in the logarithmic region for pressure driven flows.

The results for different Ra numbers are collected in table 4. The table shows the values of D_p/D_1 for different Ra numbers, different wall normal locations y, and different orders of the structure functions p.

Table 4: Overview of all data from table 3. The numbers indicate the calculated values of D_p/D_1 for the different Ra number cases at different wall normal locations. For all data, we have $\Gamma = 16$.

$y =$	0.03		0.06		0.15		0.3		0.5		
$Ra =$	10^8	10^9	10^8	10^9	10^8	10^9	10^8	10^9	2×10^7	10^8	10^9
p = 2	1.55	1.54	1.50	1.52	1.51	1.54	1.61	1.61	1.63	1.64	1.61
p = 3	1.98	1.97	1.89	1.94	1.89	1.99	2.12	2.13	2.18	2.20	2.14
p = 4	2.32	2.32	2.17	2.28	2.19	2.38	2.55	2.57	2.65	2.68	2.58
p = 5	2.54	2.57	2.38	2.55	2.42	2.70	2.92	2.95	3.06	3.10	2.97

5 Discussion

5.1 Structure function verification

In the first three sections of the results, the validity of the method for calculating the structure functions was tested. This was done in three different ways, which will be discussed in this section.

5.1.1 Dependence on aspect ratio

In the first section of the results, the second order structure functions for different aspect ratios of the domain were compared. There is a very good agreement between the different aspect ratio cases for smaller separations r. As expected, the flow at small scales is not influenced by the size of the periodic domain, which is relatively large for every case. For the large values of r, the expectation was that the structure functions reach a plateau, corresponding to an independence of r. This follows directly when r is large enough such that the velocity at that distance is uncorrelated. Due to the oscillating behavior of the structure functions, this plateau is only reached for the case where $\Gamma = 64$. The lower aspect ratios still show an oscillation for their largest values of r, so there is still a correlation in the velocity field at a separation that is half the domain width.

This latter observation is also the reason why many results are only shown for the case with $Ra = 10^8$ and $\Gamma = 64$, since that was the highest aspect ratio case available. This has two main advantages. The first advantage is that the dynamics of the large structures (size $\sim 5H$) is least influenced by the periodic boundaries of the domain. The second advantage of the $\Gamma = 64$ case is that the large domain also implies more data, since the grid resolution is the same for different aspect ratios. This reduces the confidence intervals for the structure functions, which are determined after averaging over space.

5.1.2 Large scale structures

The observed oscillations in the structure functions are a result of large scale structures in the flow, which provides a second method of varifying the structure functions. A local minimum in the structure functions at r_0 implies that the velocities at a distance r_0 are positively correlated, so there are structures of size r_0 in the flow. The size of the observed structures was compared with the energy spectrum. There is a good agreement between those two methods, since both methods indicate structures of size ~ 5.5. This also implies that the structure functions are a good method of finding structures in the velocity field, because they show the size of those structures very clearly (see figure 7). It is remarkable however that the large scale structures are not visible in the half-height plane ($y = 0.5$). Both the structure functions and the kinetic energy spectrum show no clear structure size. This makes the structure functions in the half-height plane more smooth and allows a better determination of the structure function ratios as seen when discussing the extend self similarity.

5.1.3 Comparison to expected scaling

The third method of validating the structure functions was a comparison with expected scalings in different regions. For the smallest values of r, the structure functions are shown to scale as expected as r^2. However, this scaling is only visible for $r/H < 0.02$, and it is less clear for the higher order structure functions. The reason that this scaling disappears for larger values of r is that it assumes that the velocity field changes linearly in space. That fact that the r^2 scaling can actually be observed, indicates that the grid resolution is small enough to capture the small velocity fluctuations in the flow.

In the ISR, the structure functions were expected to scale according to the exponents given by the She-Leveque model. This scaling is clearly visible in the range $0.1 < r/H < 1$. This domain is somewhat shorter near $y = 0.5$ and longer near the bottom wall. The scaling exponents from the She-Leveque differ by a small amount from the original K41 predictions, with larger deviations for higher order structure functions. The data shows that the scaling exponent is indeed lower for the higher order structure functions. This method can therefore potentially be used to verify the She-Leveque model.

For the largest separations r, the structure functions reach a value that is independent of r. This value is predicted as twice the variance of the velocity fluctuations, and is calculated independently of the structure functions. There is a good agreement between the structure functions and twice the variance for $r/H > 10$, since this is when the oscillations have died out. As discussed before, this agreement is not found for the lower aspect ratio cases.

5.2 Error estimates

In table 2 in the results, the structure functions are shown with their 95% confidence bounds indicated in grey. Two trends in these intervals are visible. Firstly, the intervals increase for larger separations. This is mainly caused by a larger correlation time for those larger values of r, since the larger structures change more slowly in time. For the time averaging process, this mean that there are less uncorrelated time samples, so the error is larger. Another trend is that the error is lower near the half-height plane ($y = 0.5$). This probably has something to do with the absence of large structures in this regime making the flow more homogeneous, but more analysis on that would be needed to explain this trend.

5.3 Self similarity

As shown by De Silva (2017) [10], the structure functions in the logarithmic region of pressure driven flow show the following self similar profile:

$$S_{2p} = D_p \ln \frac{r}{y} + E_p. \tag{26}$$

This profile could not be found in this research on Rayleigh-Bénard convection for any of the Ra numbers. There seems to be no universal profile for the structure functions as a function of r and y in the ECR. The main difference between RB convection and the cases studied so far is that there is no mean velocity profile for RB convection. This could have an impact on the longitudinal structure functions that are considered here. For the pressure driven flows, the structure functions were calculated in the direction of the mean flow. In this research, the structure functions were taken in one of the horizontal directions, orthogonal to gravity. It may be that the structure functions only show this self similarity in a boundary layer created by a strong mean flow. This has to be tested in further research.

5.4 Extended self similarity

Even though the expected self similar profile could not be observed, there is a strong indication for the extended self similarity given by:

$$S_{2p} \sim \frac{D_p}{D_1} S_1 + E_p - \frac{D_p}{D_1} E_1. \tag{27}$$

The $(2p)^{\text{th}}$ order structure functions seem to scale approximately linear with the second order structure function in the range $0.2 < r/H < 3$. Since for the $y = 0.5$ case the structure functions increase monotonously, the different orders scale linearly for $0.2 < r/H < 32$. In these linear regions, a least squares linear regression has been performed to determine the slopes.

The problem with this method is that there is no objective heuristic to determine the range where the SFs scale linearly. Looking at the graph in table 2, the lower bound was chosen as the point where S_2 exceeded half its maximum value, and the upper bound was chosen as the point where S_2 was first equal to its maximum. Between those two bounds, the linear regression was performed. A different heuristic will likely result in slightly different values of D_p/D_1.

A difference with existing literature is that data for many different wall normal locations y was used, in stead of only values in the logarithmic region. The results from this research show that the coefficients D_p/D_1 are almost constant close to the boundary ($y < 0.1$), and that they increase in the bulk region

$(0.15 < y < 0.3)$, as shown in figure 14. Interestingly, the values of D_p/D_1 seem to intersect the literature data in a small region around $y \approx 0.2$. Apparently the extended self similar coefficients D_p/D_1 are not constant for any flow field, but in stead are dependent on the wall normal distance.

The results also seem to indicate that the coefficients D_p/D_1 are independent of Ra, but more Ra numbers are required to give a definitive answer to that. The data at $y = 0.5$ however shows a very good agreement for $Ra = 10^7 - 10^9$ as shown in figure 15. This Ra is independence promising since for the half-height plane, the structure function ratios were determined relatively accurately due to small confidence intervals and a larger range where the SFs scale linearly.

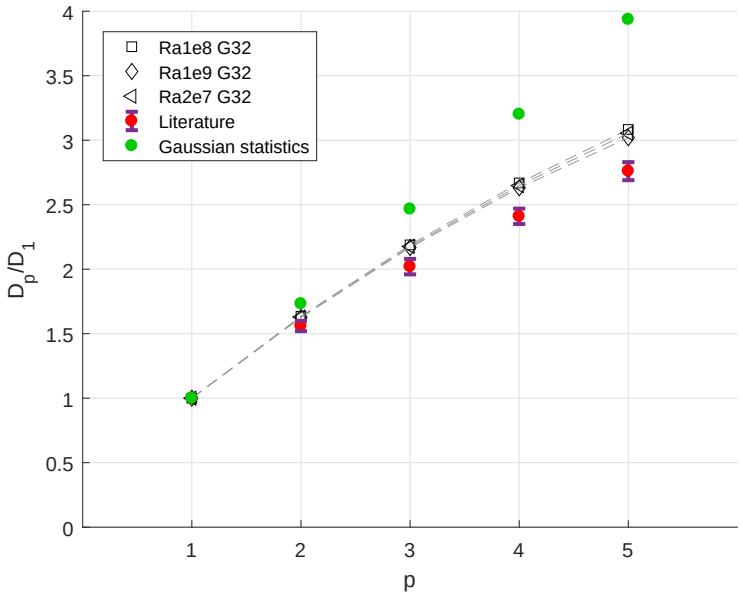

Figure 15: Extend Self Similarity for the half-height slab ($y = 0.5$). In red, the data from De Silva (2017) is shown, while the green dots represent Gaussian statistics.

6 Conclusion

- **Self Similarity (SS)**: Do the structure functions for Rayleigh-Bénard flow show the same logarithmic profile (equation 6) as for the pressure driven flows?

In contrary to the findings for pressure driven flows, the structure functions in Rayleigh-Bénard convection do not show a logarithmic self similar profile. There is no collapse to a universal profile with parameter r/y. We expect that this profile is only present in the logarithmic layer. The Ra numbers used in this research were not large enough to have a logarithmic layer. However, the structure functions for all wall normal distances show the expected scaling with r in different regions. In particular, the structure functions the predicted scaling for the dissipation range, inertial range and in the limit for large r.

- **Extended Self Similarity (ESS)**: Can the results for the structure function ratios D_p/D_1 (equation 8) for pressure driven flows be generalized to include flows driven by natural convection at different wall normal distances?

Even though the structure functions do not show the expected self similar profile, there is clear evidence for the extended self similarity coefficients D_p/D_1. These coefficients appear to be dependent on the wall normal height y, as they are higher near the half-height plane. The coefficients only agree with the literature data in a small range of wall normal heights around $y = 0.2$. This might be because in the literature, the data was taken in the logarithmic region of pressure driven flows. There are strong hints to an independence of D_p/D_1 with Ra, but further research is required to prove this.

7 Recommendations

In this research, the existence of (extended) self similar profiles in Rayleigh-Bénard convection has been studied. There are however still a lot of open question for which further research is needed to answer them. This section contains some recommendations for further research.

7.1 Higher resolution of structure functions

As described in section 3, the structure functions $S_{2p}(r)$ have only been calculated on about $n_r = 80$ different separation distances r. To more accurately examine the oscillating nature of the structure functions for large values of r, more values of r would have to be used for a better resolution.

However, the calculation time scales proportional to n_r. In order to get a higher resolution without increasing the calculation time too much, the code used in this research will have to be optimized for better parallel computing performance. With the current method, the performance decreases rapidly for larger data sets. This is because a lot of data has to be transferred to the CPUs. For the largest data sets in this research, distributing the computations to 24 CPUs yielded only about a factor of two reduction in calculation time compared to serial computing. It is therefor recommended to translate the code to Fortran, where better parallel computing toolboxes for large data structures are available.

7.2 Self similar profiles for Couette flow

In contrast to recent findings in literature on pressure driven flows, there seems to be no self similar profile in the ECR for the structure functions in RB convection according to the results from this research. The main difference with previous findings is that there is no mean velocity in RB convection. It is therefore to see the effect of a mean velocity on the structure functions. This can be done by applying the methods from this research to different cases of Couette flow. Couette flow is the flow between two parallel surfaces where the surfaces move tangentially relative to each other, creating a mean average velocity profile [12]. Also, buoyancy effects can be studied by setting a temperature difference between the plates. When the relative velocity of the plates is set to 0, this flow configuration is equivalent to RB convection. By investigating the structure functions for different configurations of Couette flow, the effect of a mean average velocity on the structure functions can be determined.

7.3 Dependence of ESS coefficients on wall normal height

It is clear from the results in this report that the ESS coefficients D_p/D_1 are dependent on the wall normal height in RB convection. Near the bottom wall, these coefficients are lower than in the bulk of the domain. There seems to be a transition in the region $0.15 < y < 0.3$. To accurately determine the dependence on y however, more data from different values of y is needed since in this research only 8 values of y were considered.

7.4 Dependence of ESS coefficients on Raleigh number

This research hints at an independence of the coefficients D_p/D_1 on the Rayleigh number. At y, the results are within 3% for the different Ra numbers. For the other wall normal heights, the coefficients will have to be determined more accurately and for a higher aspect ratio.

7.5 Temperature structure functions

So far, only the scaling of the longitudinal velocity structure functions has been considered. However, for RB convection, the same analysis can be applied to the temperature field. It would be interesting to see of the temperature also shows the extended self similarity in the ECR, and how it is connected to the velocity field [18].

Acknowledgments

I would like to thank my supervisors, Prof. Bernard Geurts and Ass. Prof. Richard Stevens, for the opportunity to do this research. Thanks to their input, I was able to combine my two fields of study in this assignment. They offered great help during my research by steering me in the right direction during our meetings, and proofreading my report.

I would also like to thank my daily supervisor, MSc. Alexander Blass, for his continuous support during my research. His door was always open when I had questions, and he offered great help in checking my results and proofreading my report. He also provided my with the necessary codes to work on Cartesius, and the energy spectra shown in this report.

Lastly, I want to thank Xiaojue Zhu for proofreading my report.

Arnout Franken

References

[1] I. Marusic, B. J. McKeon, P. A. Monkewitz, H. M. Nagib, A. J. Smits, and K. R. Sreenivasan. *Wall-bounded turbulent flows at high Reynolds numbers: Recent advances and key issues.* Phys. Fluids, **22**(6), 065103, 2010.

[2] A. J. Smits, B. J. McKeon, and I. Marusic. *High–Reynolds number wall turbulence.* Ann. Rev. Fluid Mech., **43**(1), 353, 2011.

[3] J. Jiménez. *Cascades in wall-bounded turbulence.* Ann. Rev. Fluid Mech., **44**(1), 27, 2012.

[4] A. J. Smits and I. Marusic. *Wall-bounded turbulence.* Phys. Today, **66**(9), 25, 2013.

[5] I. Marusic, J. P. Monty, M. Hultmark, and A. J. Smits. *On the logarithmic region in wall turbulence.* J. Fluid Mech., **716**, R3, 2013.

[6] R. J. A. M. Stevens, M. Wilczek, and C. Meneveau. *Large-eddy simulation study of the logarithmic law for second- and higher-order moments in turbulent wall-bounded flow.* J. of Fluid Mech., **757**, 888, 2014.

[7] C. Meneveau and I. Marusic. *Generalized logarithmic law for high-order moments in turbulent boundary layers.* J. Fluid Mech., **719**, R1, 2013.

[8] C. M. de Silva, I. Marusic, J. D. Woodcock, and C. Meneveau. *Scaling of second- and higher-order structure functions in turbulent boundary layers.* J. Fluid Mech., **769**, 654, 2015.

[9] X. I. A. Yang, C. Meneveau, I. Marusic, and L. Biferale. *Extended self-similarity in moment-generating-functions in wall-bounded turbulence at high Reynolds number.* Phys. Rev. Fluids, **1**, 044405, 2016.

[10] C.M. de Silva, D. Krug, D. Lohse, and I. Marusic. *Universality of the energy-containing structures in wall bounded turbulence.* Submitted to J. Fluid Mech., 2017.

[11] R. Benzi, S. Ciliberto, R. Tripiccione, C. Baudet, F. Massaioli, and S. Succi. *Extended self-similarity in turbulent flows.* Phys. Rev. E, **48**, 29, 1993.

[12] P. K. Kundu, I. M. Cohen, and D. R. Dowling. *Fluid Mechanics.* Elsevier Science, 6th edition, 2016.

[13] R. P. J. Kunnen, H. J. H. Clercx, B. J. Geurts, L. J. A. van Bokhoven, R. A. D. Akkermans, and R. Verzicco. *Numerical and experimental investigation of structure-function scaling in turbulent Rayleigh-Bénard convection.* Phys. Rev. E, **77**, 016302, 2008.

[14] F. Anselmet, Y. Gagne, E. J. Hopfinger, and R. A. Antonia. *High-order velocity structure functions in turbulent shear flows.* J. Fluid Mech., **140**, 63, 1984.

[15] Z. She and E. Leveque. *Universal scaling laws in fully developed turbulence.* Phys. Rev. Lett., **72**, 336, 1994.

[16] R. J. A. M. Stevens, A. Blass, X. Zhu, R. Verzicco, and D. Lohse. *Superstructures in Rayleigh-Bénard convection.* To be submitted.

[17] T. Hartlep, A. Tilgner, and F. H. Busse. *Large scale structures in Rayleigh-Bénard convection at high Rayleigh numbers.* Phys. Rev. Lett., **91**, 064501, 2003.

[18] G. Ruiz Chavarria, C. Baudet, and S. Ciliberto. *Extended self-similarity of passive scalars in fully developed turbulence.* Europhys. Let., **32**(4), 319, 1995.